LETTER

doi:10.1038/nature20601

Correlated fluorescence blinking in two-dimensional semiconductor heterostructures

Weigao Xu[1], Weiwei Liu[1], Jan F. Schmidt[2], Weijie Zhao[1], Xin Lu[1], Timo Raab[2], Carole Diederichs[3,4], Weibo Gao[1], Denis V. Seletskiy[2] & Qihua Xiong[1,4,5]

'Blinking', or 'fluorescence intermittency', refers to a random switching between 'ON' (bright) and 'OFF' (dark) states of an emitter; it has been studied widely in zero-dimensional quantum dots[1] and molecules[2,3], and scarcely in one-dimensional systems[4,5]. A generally accepted mechanism for blinking in quantum dots involves random switching between neutral and charged states[6,7] (or is accompanied by fluctuations in charge-carrier traps[8]), which substantially alters the dynamics of radiative and non-radiative decay. Here, we uncover a new type of blinking effect in vertically stacked, two-dimensional semiconductor heterostructures[9], which consist of two distinct monolayers of transition metal dichalcogenides (TMDs) that are weakly coupled by van der Waals forces. Unlike zero-dimensional or one-dimensional systems, two-dimensional TMD heterostructures show a correlated blinking effect, comprising randomly switching bright, neutral and dark states. Fluorescence cross-correlation spectroscopy analyses show that a bright state occurring in one monolayer will simultaneously lead to a dark state in the other monolayer, owing to an intermittent interlayer carrier-transfer process. Our findings suggest that bilayer van der Waals heterostructures provide unique platforms for the study of charge-transfer dynamics and non-equilibrium-state physics, and could see application as correlated light emitters in quantum technology.

During the past two decades, quantum dots have been invoked as a classical model system for understanding the blinking effect[1,6,8]. Owing to the puzzling nature of blinking—and the need for effective strategies to produce non-blinking quantum dots[10]—several different types of models[4] have been developed to explain the physical origins of the effect. However, controversial reports notwithstanding[11,12], a generally accepted underlying mechanism is the random switching between neutral states (ON periods) and charged states (OFF periods, characterized by the non-radiative Auger effect), driven by charge transfer[6,8]. For zero-dimensional (0D) or one-dimensional (1D) systems, emission properties are highly related to the charge state of the surface. But for bulk fluorescent materials, the surface state no longer makes a dominant contribution to the overall emission, and thus the blinking effect is usually absent.

Monolayer two-dimensional (2D) TMD semiconductors have emerged as promising systems in fundamental and technologically relevant studies of valleytronic, electronic and optoelectronic devices, whose unique properties are enabled by inversion symmetry breaking and strong spin–orbit coupling[13]. Such monolayers usually exhibit strong excitonic emission, in which neutral and charged excitons have been well characterized; the relative intensity and emission energy of the excitons are sensitive to the injection of holes/electrons with gate modulation[14,15]. Although surface state is crucial to the emission properties, most 2D monolayer emitters have been found to emit light with stable intensity[16]. This might be due to an equilibrium charge-transfer state (if any), leading to non-blinking emission.

2D heterostructures that are stacked vertically in Lego-like fashion provide additional knobs by which to manipulate the charge dynamics, leading to unprecedented functionalities that are beyond the reach of any single component; for example, these heterostructures can act as tunnelling field-effect transistors[17], as light-emitting diodes[18], or in interlayer exciton valleytronic applications[19,20]. This variety of functions results from a variety of dielectric confinements or from a unique charge-transfer mechanism that is enabled by the staggered band alignment. Here we demonstrate that vertically stacked bilayer heterostructures exhibit a new fluorescence blinking effect. Unlike the random switching that occurs between pristine and dark states (or between several dark states[21,22], owing to multiple charge states and recombination pathways) in 0D and 1D systems, the blinking effect in 2D heterostructures exhibits a correlated switching between two monolayers, leading to blinking between bright, neutral and dark states (Fig. 1a), with the bright and dark states in each of the two monolayers being negatively correlated.

Figure 1b shows an optical image of an as-prepared $WS_2/MoSe_2$ bilayer heterostructure (see Methods). The monolayer characteristic of the components of 2D heterostructures can be seen in optical contrast and confirmed through the identification of low-frequency vibrational fingerprints in Raman scattering[23] and emission features (see Supplementary Information and Supplementary Figs 1, 2). The absence of the interlayer breathing mode[23] in most as-prepared bilayer heterostructures suggests a weak interlayer interaction. Figure 1c–e displays three fluorescence images of the heterostructure, taken with a colour charge-coupled-device camera at different times, and clearly indicating distinct bright, neutral and dark states for WS_2 emission at the heterostructure region. We also used a high-speed camera to record the emission dynamics of the heterostructures; representative snapshots are shown in Fig. 1f, g, and correspond to the dynamical emission of A excitons from WS_2 (Fig. 1f) and from $MoSe_2$ (Fig. 1g; see Methods). Video clips of WS_2 and $MoSe_2$ emissions are provided in Supplementary Videos 1 and 2. In accordance with the literature[16], we find that monolayers of WS_2 (Fig. 1h, black trace) or $MoSe_2$ (Fig. 1i, black trace) emit light with almost constant intensity over time. But the emission intensity at the heterostructure region shows a typical blinking behaviour (see Fig. 1h, i, red traces, and statistical analyses of state distributions in Supplementary Fig. 4). This is intriguing given that most studies of emission in 2D heterostructures uncovered a quenching effect as compared with monolayer emitters[19,24–27].

According to the band alignment (see Supplementary Fig. 5), WS_2 and $MoSe_2$ monolayers form a heterojunction with a staggered gap, different to that in the typical fluorescence resonance energy transfer model[28] (with a straddling gap). When the two monolayers are near each other, the electrons excited in $MoSe_2$ tend to move and accumulate at the conduction band of WS_2, while the

[1]Division of Physics and Applied Physics, School of Physical and Mathematical Sciences, Nanyang Technological University, 637371 Singapore. [2]Department of Physics and Center for Applied Photonics, University of Konstanz, D-78457 Konstanz, Germany. [3]Laboratoire Pierre Aigrain, Ecole Normale Supérieure, PSL Research University, CNRS, Université Pierre et Marie Curie, Sorbonne Universités, Université Paris Diderot, Sorbonne Paris-Cité, 24 Rue Lhomond, 75231 Paris Cedex 05, France. [4]MajuLab, CNRS–UNS–NUS–NTU International Joint Research Unit, UMI 3654 Singapore. [5]NOVITAS, Nanoelectronics Center of Excellence, School of Electrical and Electronic Engineering, Nanyang Technological University, 639798 Singapore.

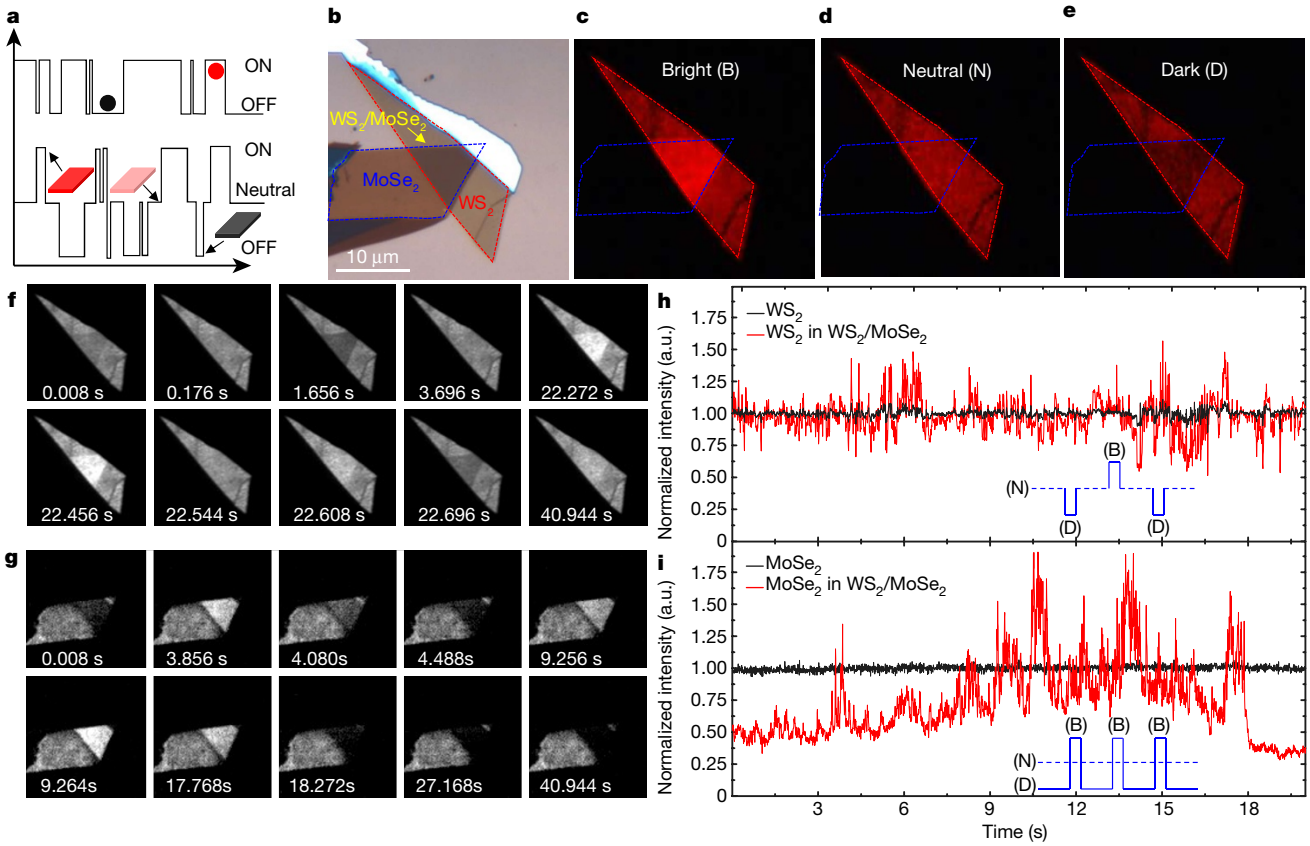

Figure 1 | Fluorescence blinking in a loosely contacted $WS_2/MoSe_2$ 2D bilayer heterostructure. a, Illustrations of a typical blinking quantum dot (top; with ON/OFF states) and a blinking 2D bilayer heterostructure (bottom; with bright/neutral/dark states). **b**, Optical image of a trapezoidal $WS_2/MoSe_2$ bilayer heterostructure, formed by aligned stacking of a WS_2 monolayer and a $MoSe_2$ monolayer. **c**–**e**, Fluorescence image taken with a colour camera at different times, showing a bright (**c**), neutral (**d**) and dark (**e**) emission state of WS_2 at the $WS_2/MoSe_2$ junction. The exposure time was 50 ms. **f**, **g**, Snapshots of representative fluorescence images at different times, showing emission from WS_2 (**f**) and $MoSe_2$ (**g**); the exposure time for each frame was 8 ms. **h**, **i**, Time traces showing variations in emission intensity for: **h**, a WS_2 monolayer alone (black trace) or within a $WS_2/MoSe_2$ bilayer (red trace); and **i**, a $MoSe_2$ monolayer alone (black trace) or within a $WS_2/MoSe_2$ bilayer (red trace), over a time period of 20 s. These traces were calculated from the greyscale of frames from two videos recorded with a high-speed camera, with a 645-nm bandpass filter for WS_2 (**h**) and a 794-nm bandpass filter for $MoSe_2$ (**i**).

holes excited in WS_2 will accumulate at the valence band of $MoSe_2$, possibly on an ultrafast timescale for closely contacted monolayers[24]. Figure 2a shows a model of a neutral state with negligible interlayer carrier transfer; here, the emission feature of the heterostructure will be similar to the combined emission spectrum of two individual monolayers. However, we hypothesize that, if net electrons are injected from the conduction band of the electron donor to the electron acceptor, this 'electron-dominated' carrier-transfer process will cause a bright (or dark) state of the electron acceptor (or donor) (Fig. 2b); meanwhile, if net holes are injected from the valence band of the electron acceptor to the electron donor, this 'hole-dominated' carrier-transfer process will lead to a dark (or bright) state of the electron acceptor (or donor) (Fig. 2c). If the two processes occur simultaneously, emission of both $MoSe_2$ and WS_2 will be quenched, leading to a probable interlayer exciton emission (Fig. 2d), as previously observed in a few combinations[19,26]. Meanwhile, for a loosely contacted vertical bilayer junction, the charge-transfer channel might be partially blocked, resulting in unbalanced electron/hole transfer. We refer to our model as 'intermittent interlayer carrier transfer' (IICT). We anticipate that the blinking behaviour of these heterostructures originates from random switching between these different kinds (and different degrees) of charge-transfer states. We have observed blinking phenomena in five out of six possible bilayer heterostructure combinations (see Supplementary Information and Supplementary Figs 5–10), suggesting that the IICT process is a general phenomenon in 2D TMD heterostructures.

To probe the actual charge-transfer dynamics, we studied the transient absorption spectroscopy of a $MoSe_2/WSe_2$ heterostructure with two distinct regions of charge-transfer state (see Fig. 2e for optical and fluorescence images)—that is, a near-neutral region (charge-transfer state 'a') and a darker region (charge-transfer state 'd'; see Methods and Supplementary Fig. 3 for more details). Our results indicate that, in the darker region, there is an ultrafast charge-transfer timescale of about 120 fs (indicated by the vertical black lines); in the near-neutral region, charge transfer is much weaker (Fig. 2f, g).

A loose contact state is essential in the IICT model, allowing the selective opening of electron/hole transport channels. We anticipate that incident light excites electrons and holes in both monolayers, and that, after a certain degree of carrier accumulation, the built-in electrical field between the two monolayers drives an interlayer carrier-transfer process (possibly through interlayer tunnelling or hopping). Such cycles of accumulation, tunnelling, accumulation, and so on produce patterns of bright, neutral and dark emission in a 2D heterostructure. This IICT model predicts that: first, the intensity and energy of neutral and (positively or negatively) charged exciton emission are altering owing to dynamic charge transfer; and second, the intensity and dynamics of exciton emission in two components exhibit negative correlations in time.

We further studied the emission spectra as a function of time during the blinking process, in order to unravel the dynamics of the intermittent charge transfer. Interlayer carrier transfer in a bilayer heterostructure will change the degree of doping in both monolayers,

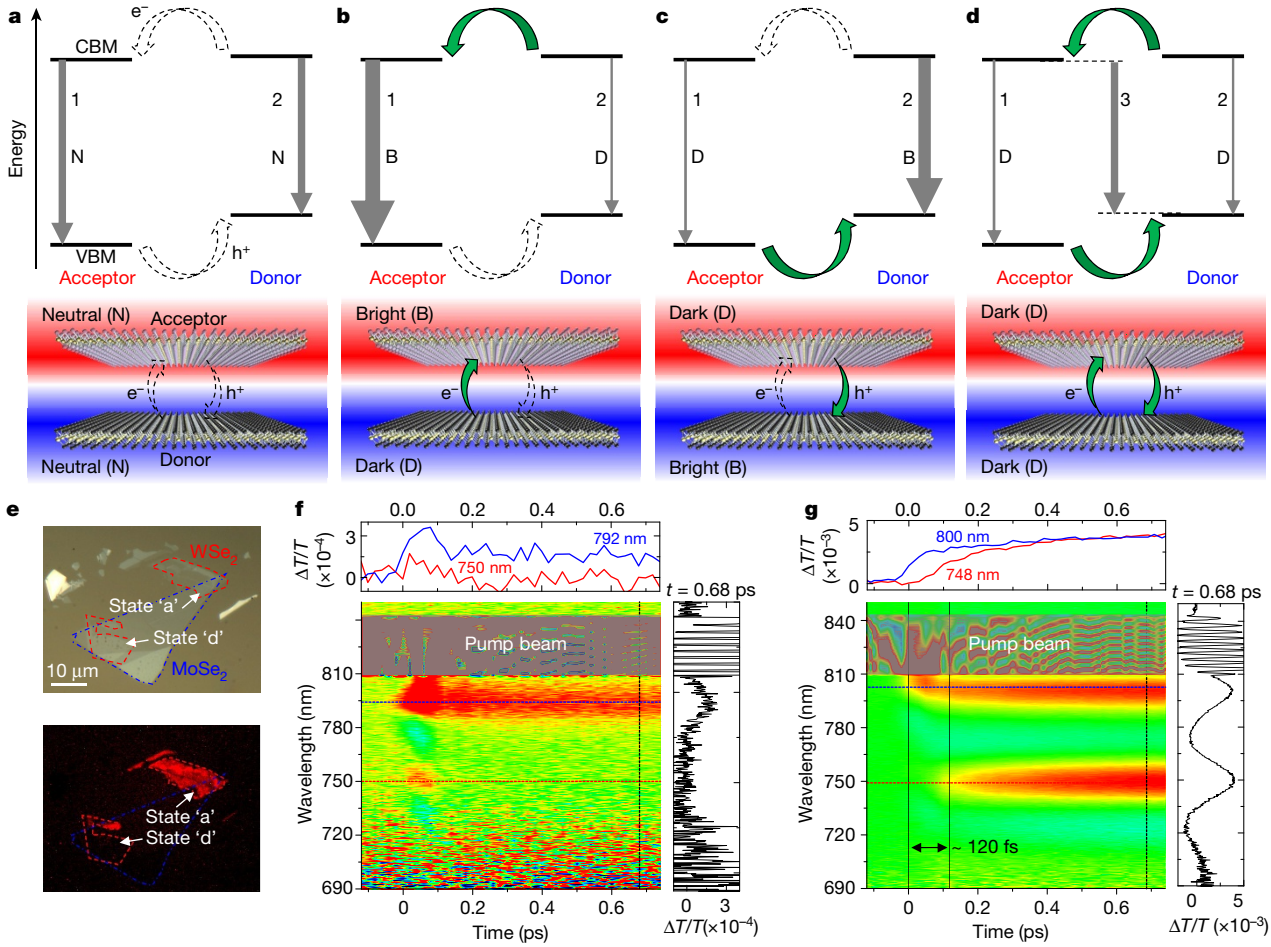

Figure 2 | The IICT model of fluorescence blinking in 2D heterostructures. a, A neutral state. Top, band alignment showing the conduction band minimum (CBM) and valence band maximum (VBM) of a typical bilayer TMD heterostructure, with one component acting as an electron donor (for example, $MoSe_2$ in $WS_2/MoSe_2$) and its counterpart as an electron acceptor (for example, WS_2 in $WS_2/MoSe_2$). Grey arrows indicate the emission of an A-exciton from the electron acceptor (1) and from the electron donor (2). Bottom, diagram showing the junction between the monolayers in the TMD heterostructure. e^-, electron; h^+, hole. **b**, An electron-dominated carrier-transfer process, which will result in a dark emission state in the electron donor and a bright state in the electron acceptor. **c**, A hole-dominated carrier-transfer process, which will result in a bright emission state in the electron donor and a dark state in the electron acceptor. **d**, A bilayer heterostructure with unimpeded carrier-transfer channels (for both electrons and holes). Emission from electron donor and acceptor will be quenched. This process will probably appear when the two monolayers of the bilayer are in close contact, and will allow emission of an interlayer exciton (3). **e–g**, Transient absorption measurements from a $MoSe_2/WSe_2$ heterostructure. **e**, Optical (top) and fluorescence (bottom) images, showing a near-neutral region (state 'a') and a darker region (state 'd'). **f**, **g**, Pump–probe measurements for the near-neutral region (**f**) and the dark region (**g**). In the main panels, the normalized differential transmission ($\Delta T/T(\lambda,t)$) of the broadband 13-fs probe beam is depicted in two-dimensional false-colour maps versus the pump–probe delay time and the wavelength. In both cases, the spectrum of the 60-fs excitation pulse (810 nm to 845 nm) is adjusted to overlap with the absorption of $MoSe_2$ monolayer. The top panels depict the signal dynamics evaluated at fixed wavelengths, indicated on the colour maps with horizontal colour-coded dashed lines. The right panels depict dynamic spectral signatures of the signal evaluated at fixed delay times t and indicated by black vertical dashed lines.

affecting their neutral and charged exciton emission features[14]. We first examined the time-dependent spectral features of a blinking MoS_2/WS_2 bilayer in which WS_2 is an electron donor (and MoS_2 is an electron acceptor). Figure 3a shows typical spectra from WS_2 emission in the heterostructure region, revealing a brighter state (but weaker than that seen with WS_2 alone; see Methods and Supplementary Video 3) at 73.2 seconds (top frame) and a darker state at 76.8 seconds (bottom frame). We fitted the spectra with two Gaussians, for neutral exciton and trion emission. Our pristine WS_2 layer is an n-type semiconductor, which emits neutral excitons (X^0) as well as negatively charged trions (X^-). Electron emigration and hole accumulation lead to a more positively (less negatively) charged WS_2 (while hole accumulation is minor, as more dark states were observed). Figure 3b (top) shows how the integrated intensity and the intensity ratio X^+/X^0 varies with time. The two curves show a mirror symmetry, suggesting that the WS_2 in MoS_2/WS_2 heterostructures is no longer n-type (polarity has reversed, possibly owing to an initial balanced charge transfer); otherwise, the X^-/X^0 ratio for n-type WS_2 would decrease with decreased intensity (because electron emigration in a dark state makes the WS_2 layer less negative).

Furthermore, the IICT process also induces a time-dependent shift in the emission energy of the MoS_2/WS_2 bilayer—that is, a small blueshift in the X^0 emission (within 1 meV) and a pronounced redshift in the X^+ emission (which can reach 7 meV) during switching between a weaker and a darker state (Fig. 3b, bottom). The change in excitonic energy results from the combined effect of band-structure renormalization and band filling (see Supplementary Information and Supplementary Fig. 9). Figure 3 shows state-distribution diagrams that plot intensity versus the X^+/X^0 (X^-/X^0 for bare WS_2) ratio (Fig. 3c), and intensity versus emission energy (Fig. 3d), for MoS_2/WS_2. Data from a bare WS_2 region (which is non-blinking) are plotted for comparison. The range of intensities is much greater for the heterostructure versus the bare WS_2; moreover, we can see a monotonous dependence in the

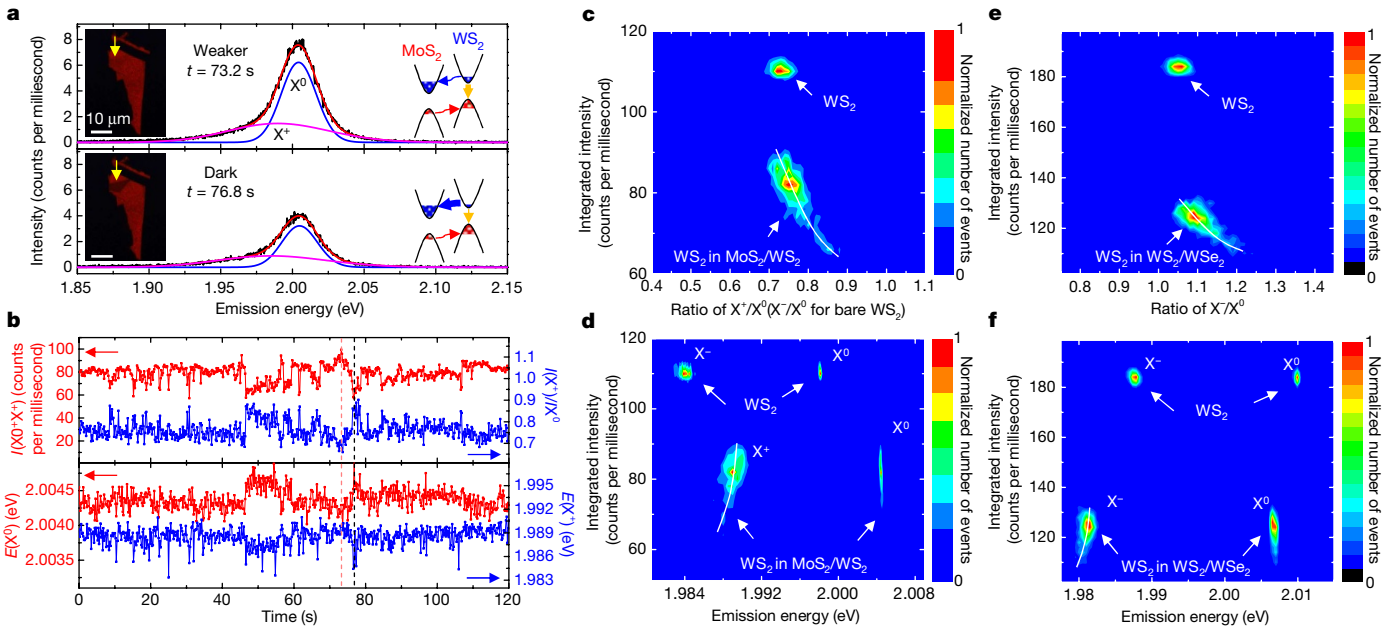

Figure 3 | Variation in trion and exciton emission from heterostructures over time. Emission was monitored from a WS_2 monolayer in blinking MoS_2/WS_2 and WS_2/WSe_2 bilayer heterostructures. X^0, neutral exciton; X^+, positively charged trion; X^-, negatively charged trion. **a**, Typical emission spectra, with Gaussian fitting, from a blinking MoS_2/WS_2 heterojunction: top, a brighter state (but less bright, or weaker, than that produced by emission from bare WS_2); bottom, a darker state. The left insets are representative fluorescence images. The right insets are illustrations of different carrier-transfer states, showing slight electron transfer (top, thin blue line) and strong electron transfer (bottom, thick blue line). **b**, Top, time trace of integrated total emission intensity from WS_2 in MoS_2/WS_2 ($I(X^0+X^+)$; red curve), and time trace of the intensity ratio of trion/exciton emission ($I(X^+)/I(X^0)$) from WS_2 in MoS_2/WS_2 (blue curve). Bottom, time traces of emission energy from neutral exciton emission ($E(X^0)$; red curve) and trion emission ($E(X^+)$; blue curve). Red and black vertical dashed lines indicate $t = 73.2$ seconds and $t = 76.8$ seconds, respectively. **c**, **d**, Statistical analyses of state distribution on the basis of the time traces in **b**, allowing visualization of the relationship between emission intensity and the trion/exciton ratio (**c**), and of the relationship between emission intensity and emission energy (**d**). Data from an isolated WS_2 region are plotted for reference. **e**, **f**, Similar state distribution of WS_2 emission from a blinking WS_2/WSe_2 bilayer heterojunction, the main difference being that X^+ emission is replaced with X^- emission, because WS_2 becomes an electron acceptor in WS_2/WSe_2. All spectra were taken with a 50-ms exposure, with an interval of 150 ms in MoS_2/WS_2 and of 50 ms in WS_2/WSe_2. All excitation was carried out with a 532-nm continuous wave laser.

intensity versus X^+/X^0 ratio and in the intensity versus X^+ emission energy at the blinking region (see the white lines in Fig. 3c, d).

We then examined a blinking WS_2/WSe_2 bilayer heterojunction in which WS_2 acts as an electron acceptor. We found that intermittent electron injection and hole emigration (dominating) cause even higher n-doping of the WS_2 layer, resulting in a larger X^-/X^0 ratio and redshifted X^- emission (as compared with its pristine monolayer component) in a dark state (Fig. 3e–f and Supplementary Fig. 8). The dynamic fluctuations in the ratios of trions to neutral excitons—and the variations in emission energy—are in agreement with the intermittent interlayer carrier-exchange process.

We then carried out steady-state and time-resolved fluorescence cross-correlation spectroscopy, in order to understand in depth the physical mechanism underlying blinking in the 2D system. Such measurements allow us to monitor the time dependence of the emission characteristics of both donor and acceptor, simultaneously but separately. To unravel the possible correlation between the two components in an emitter pair (for example, $WS_2/MoSe_2$), we evaluated the cross-correlation function that is defined as:

$$G(\tau) = \frac{\langle \delta I_{WS_2}(t) \cdot \delta I_{MoSe_2}(t+\tau) \rangle}{\langle I_{WS_2}(t) \rangle \cdot \langle I_{MoSe_2}(t) \rangle} = \frac{\langle I_{WS_2}(t) \cdot I_{MoSe_2}(t+\tau) \rangle}{\langle I_{WS_2}(t) \rangle \cdot \langle I_{MoSe_2}(t) \rangle} - 1$$

where $G(\tau)$ is the cross-correlation function; I is the signal intensity with the largest occurrence in the signal-level distribution; t is time; and τ refers to the time delay of correlation (see Methods for more details). As shown in Fig. 4a–c, we carried out steady-state photoluminescence spectroscopy of a blinking $WS_2/MoSe_2$ heterostructure, in which the emission of WS_2 and $MoSe_2$ can be recorded simultaneously (see Methods). The mirror symmetry of the intensity versus time trace (Fig. 4b) and the $G(\tau)$ dip (Fig. 4c) at zero time delay suggests a prominent negative correlation between the WS_2 and $MoSe_2$ components of the emitter pair.

To further understand the blinking dynamics and accompanying physical characteristics, we carried out time-resolved fluorescence imaging and correlation experiments with the same heterostructure, using the Hanbury Brown and Twiss interferometer set-up (see Fig. 4d and Methods). Fluorescence lifetime imaging microscopy analyses (Fig. 4e, f) reveal an average fluorescence lifetime of 0.93 ns in the $WS_2/MoSe_2$ heterostructure region, which is greater than that in the isolated WS_2 monolayer (0.45 ns) but less than that in the isolated $MoSe_2$ monolayer (2.38 ns), indicating that multiple recombination processes occur in the heterostructure. The much longer fluorescence lifetime in $MoSe_2$ might be due to this monolayer's near-neutral state in ambient conditions, in which the intensity ratio of charged to neutral exciton emission is small.

We also measured emission intensities and fluorescence lifetime trajectories from $MoSe_2$ and WS_2 in the heterostructure (see Methods; Fig. 4g shows a 40-second snapshot, while Supplementary Fig. 13 shows the full 120-second time frame). The results indicate a pronounced mirror symmetry (negative correlation) in both intensity and lifetime. The $G(\tau)$ result is shown in Fig. 4h, fitted with the function $G(\tau) = A + \sum_{i=1} B_i \exp(-\tau/T_i)$, (where A, B_i and T_i are constant parameters; see Fig. 4), owing to the fact that the blinking effect is related to several dynamic processes (electron states) in the heterostructures, according to our IICT model[29]. The negative amplitude of the resulting $G(\tau)$ value corresponds to a clear negative correlation, further suggesting the intermittent carrier-exchange dynamics between the $MoSe_2$ and WS_2 monolayers, as proposed in our IICT model.

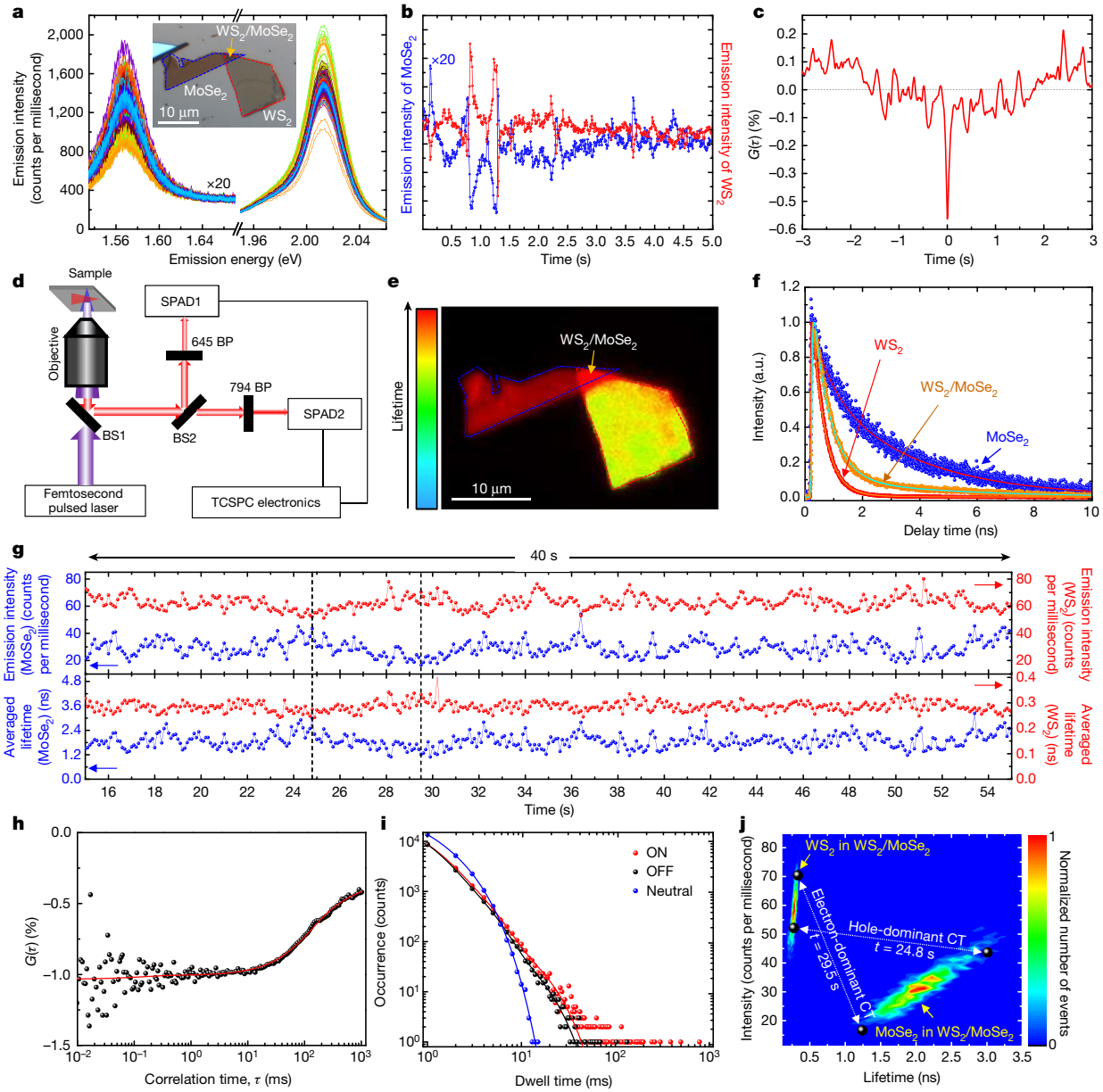

Figure 4 | Fluorescence cross-correlation spectroscopy analyses of a blinking $WS_2/MoSe_2$ bilayer heterostructure. a, Simultaneous recording of spectra for WS_2 and $MoSe_2$ emission, using a 150 lines mm^{-1} grating on an HR Evolution spectrometer. Each spectrum has an exposure time of 5 ms, and the time interval between two acquisitions is 3.7 ms. The inset shows an optical image of the $WS_2/MoSe_2$ bilayer heterostructure sample. **b**, Time-dependent intensity fluctuations of WS_2 (red curve) and $MoSe_2$ (blue curve) emission from the spectra shown in **a**. **c**, $G(\tau)$ calculated from the time-trace data in **b**, indicating a prominent negative correlation at time zero. **d**, Set-up for measuring the time-resolved fluorescence correlation. BS, beam splitter; BP, bandpass filter centred at the indicated frequencies; SPAD, single-photon avalanche diode detector; TCSPC, time-correlated single-photon counting. **e**, Fluorescence lifetime imaging microscopic image of the same $WS_2/MoSe_2$ heterostructure. **f**, Time-decay traces for the monolayer WS_2 region, the monolayer $MoSe_2$ region, and the heterostructure region. **g**, A 40-second period of emission trajectories (Top, intensity versus time; bottom, averaged lifetime versus time) for $MoSe_2$ and WS_2 in the heterostructure, measured simultaneously by two SPADs. Binning time is 100 ms. **h**, $G(\tau)$ calculated from the intensity traces shown in **g**, showing a negative correlation. The data are fitted with $G(\tau) = A + \sum_{i=1} B_i \exp(-\tau/T_i)$, where $T_1 = 378$ ms and $T_2 = 88.6$ ms. **i**, ON/neutral/OFF probability analysis of the blinking dynamics. The ON/OFF distributions are fitted with a multi-exponential model, $P(t_{ON/OFF}) = \sum_{i=1} A_i \exp(-t_{ON/OFF}/\tau_i)$, where $\tau_1 = 8.4$ ms, $\tau_2 = 1.9$ ms and $\tau_3 = 0.62$ ms for the ON times; and $\tau_1 = 7.5$ ms, $\tau_2 = 1.8$ ms and $\tau_3 = 0.58$ ms for the OFF times. The neutral distribution is fitted with a truncated power law, $P(t_{neutral}) = At^{-\alpha}\exp(-t/\beta)$ with $\alpha = 0.48$ and $\beta = 1.6$ ms. **j**, Statistical analysis of the correlated state distribution deduced from the data in **g** (and Supplementary Fig. 13), suggesting a typical hole-dominant charge transfer (CT) state (at $t = 24.8$ s) and a typical electron-dominant CT state (at $t = 29.5$ s).

We further analysed the blinking dynamics of the ON/neutral/OFF states (see Fig. 4i and Methods). The ON and OFF probability distributions each satisfy a multi-exponential model:

$$P(t_{ON/OFF}) = \sum_{i=1} A_i \exp(-t_{ON/OFF}/\tau_i),$$

while the probability distribution of the neutral state can be best fitted with a truncated power law:

$$P(t_{neutral}) = At^{-\alpha}\exp(-t/\beta)$$

(where α and β are constant parameters; see Fig. 4). This suggests that the blinking emission observed in the heterostructures might result

from a multiple-recombination process, as in the model described in ref. 30. Figure 4j displays the correlated intensity-versus-lifetime distribution of the total excitonic emission from the two monolayers. Dashed arrows mark the correlated emission of $MoSe_2$ and WS_2 at specific times; the state-distribution results suggest a possible hole-dominated carrier-transfer process at 24.8 seconds and an electron-dominated carrier-transfer process at 29.5 seconds. The statistics reveal that both the lifetime and the intensity of the two components of the heterostructure junction exhibit a negative correlation. The monotonous variation in lifetime during blinking agrees with the A-type blinking model seen in the quantum-dot system[8]. Owing to the increased radiative recombination seen in an electron-dominated carrier-transfer process, the radiative lifetime of the electron acceptor will become longer while that of the electron donor will be correspondingly shorter. Further details can be found in the Supplementary Information and Supplementary Figs 11–16.

In summary, we have uncovered a correlated blinking phenomenon in bilayer 2D semiconductor heterostructures, in which a dynamic variation in exciton emission is related to intermittent and random interlayer carrier transfer. The physical origin of this phenomenon is essentially different to that reported for 0D/1D blinking, and emission from one blinking monolayer of the heterostructure correlates negatively with emission from the other monolayer. Owing to their exotic valley-related physical properties, 2D TMD heterostructures could see application in photon detectors, ultralow threshold lasers and optoelectronic devices with valley functionalities; further understanding of interlayer charge transfer underpins the rational tailoring of multicomponent heterostructures, which will provide systems to study collective exciton phenomenon and even correlated quantum emitters.

Online Content Methods, along with any additional Extended Data display items and Source Data, are available in the online version of the paper; references unique to these sections appear only in the online paper.

Received 24 May; accepted 28 October 2016.
Published online 14 December 2016.

1. Nirmal, M. *et al.* Fluorescence intermittency in single cadmium selenide nanocrystals. *Nature* **383,** 802–804 (1996).
2. Dickson, R. M., Cubitt, A. B., Tsien, R. Y. & Moerner, W. E. On/off blinking and switching behaviour of single molecules of green fluorescent protein. *Nature* **388,** 355–358 (1997).
3. Bout, D. A. V. *et al.* Discrete intensity jumps and intramolecular electronic energy transfer in the spectroscopy of single conjugated polymer molecules. *Science* **277,** 1074–1077 (1997).
4. Frantsuzov, P., Kuno, M., Jankó, B. & Marcus, R. A. Universal emission intermittency in quantum dots, nanorods and nanowires. *Nat. Phys.* **4,** 519–522 (2008).
5. Protasenko, V., Gordeyev, S. & Kuno, M. Spatial and intensity modulation of nanowire emission induced by mobile charges. *J. Am. Chem. Soc.* **129,** 13160–13171 (2007).
6. Efros, A. L. & Rosen, M. Random telegraph signal in the photoluminescence intensity of a single quantum dot. *Phys. Rev. Lett.* **78,** 1110–1113 (1997).
7. Efros, A. L. & Nesbitt, D. J. Origin and control of blinking in quantum dots. *Nat. Nanotechnol.* **11,** 661–671 (2016).
8. Galland, C. *et al.* Two types of luminescence blinking revealed by spectroelectrochemistry of single quantum dots. *Nature* **479,** 203–207 (2011).
9. Geim, A. K. & Grigorieva, I. V. Van der Waals heterostructures. *Nature* **499,** 419–425 (2013).
10. Ji, B. T. *et al.* Non-blinking quantum dot with a plasmonic nanoshell resonator. *Nat. Nanotechnol.* **10,** 170–175 (2015).
11. Rosen, S., Schwartz, O. & Oron, D. Transient fluorescence of the off state in blinking CdSe/CdS/ZnS semiconductor nanocrystals is not governed by Auger recombination. *Phys. Rev. Lett.* **104,** 157404 (2010).
12. Zhao, J., Nair, G., Fisher, B. R. & Bawendi, M. G. Challenge to the charging model of semiconductor-nanocrystal fluorescence intermittency from off-state quantum yields and multiexciton blinking. *Phys. Rev. Lett.* **104,** 157403 (2010).
13. Xiao, D., Liu, G. B., Feng, W. X., Xu, X. D. & Yao, W. Coupled spin and valley physics in monolayers of MoS_2 and other group-VI dichalcogenides. *Phys. Rev. Lett.* **108,** 196802 (2012).
14. Mak, K. F. *et al.* Tightly bound trions in monolayer MoS_2. *Nat. Mater.* **12,** 207–211 (2013).
15. Ross, J. S. *et al.* Electrical control of neutral and charged excitons in a monolayer semiconductor. *Nat. Commun.* **4,** 1474 (2013).
16. Peimyoo, N. *et al.* Nonblinking, intense two-dimensional light emitter: monolayer WS_2 triangles. *ACS Nano* **7,** 10985–10994 (2013).
17. Britnell, L. *et al.* Field-effect tunneling transistor based on vertical graphene heterostructures. *Science* **335,** 947–950 (2012).
18. Withers, F. *et al.* Light-emitting diodes by band-structure engineering in van der Waals heterostructures. *Nat. Mater.* **14,** 301–306 (2015).
19. Rivera, P. *et al.* Observation of long-lived interlayer excitons in monolayer $MoSe_2$-WSe_2 heterostructures. *Nat. Commun.* **6,** 6242 (2015).
20. Rivera, P. *et al.* Valley-polarized exciton dynamics in a 2D semiconductor heterostructure. *Science* **351,** 688–691 (2016).
21. Park, Y. S., Bae, W. K., Pietryga, J. M. & Klimov, V. I. Auger recombination of biexcitons and negative and positive trions in individual quantum dots. *ACS Nano* **8,** 7288–7296 (2014).
22. Sampat, S. *et al.* Multistate blinking and scaling of recombination rates in individual silica-coated CdSe/CdS nanocrystals. *ACS Photonics* **2,** 1505–1512 (2015).
23. Zhao, Y. Y. *et al.* Interlayer breathing and shear modes in few-trilayer MoS_2 and WSe_2. *Nano Lett.* **13,** 1007–1015 (2013).
24. Hong, X. P. *et al.* Ultrafast charge transfer in atomically thin MoS_2/WS_2 heterostructures. *Nat. Nanotechnol.* **9,** 682–686 (2014).
25. Lui, C. H. *et al.* Observation of interlayer phonon modes in van der Waals heterostructures. *Phys. Rev. B* **91,** 165403 (2015).
26. Tongay, S. *et al.* Tuning interlayer coupling in large-area heterostructures with CVD-grown MoS_2 and WS_2 monolayers. *Nano Lett.* **14,** 3185–3190 (2014).
27. Yu, Y. F. *et al.* Equally efficient inter layer exciton relaxation and improved absorption in epitaxial and nonepitaxial MoS_2/WS_2 heterostructures. *Nano Lett.* **15,** 486–491 (2015).
28. Helms, V. *Fluorescence Resonance Energy Transfer* (Wiley-VCH, 2008).
29. Widengren, J., Mets, Ü. & Rigler, R. Fluorescence correlation spectroscopy of triplet states in solution: a theoretical and experimental study. *J. Phys. Chem.* **99,** 13368–13379 (1995).
30. Frantsuzov, P. A., Volkan-Kacso, S. & Janko, B. Model of fluorescence intermittency of single colloidal semiconductor quantum dots using multiple recombination centers. *Phys. Rev. Lett.* **103,** 207402 (2009).

Supplementary Information is available in the online version of the paper.

Acknowledgements We thank Professor C.-D. Ohl for providing us with a high-speed camera for dynamical fluorescence imaging. Q.X. acknowledges the support of the Singapore National Research Foundation through an Investigatorship award (NRF-NRFI2015-03), and the Singapore Ministry of Education via two AcRF Tier 2 grants (MOE2012-T2-2-086 and MOE2015-T2-1-047). W.L. acknowledges scholarship support from the China Scholarship Council (no. 201506160035).

Author Contributions W.X. and Q.X. designed the research; W.X., W.L. and X.L. prepared the heterostructures and carried out steady-state/transient fluorescence spectroscopy measurements and correlation measurements; J.F.S., W.Z., T.R. and D.V.S. performed transient absorption spectroscopy measurements; W.X., W.L., X.L., W.Z., J.F.S., D.V.S., C.D., W.G. and Q.X. analysed the data; and W.X., W.L. and Q.X. wrote the manuscript. All authors commented on the manuscript.

Author Information Reprints and permissions information is available at www.nature.com/reprints. The authors declare no competing financial interests. Readers are welcome to comment on the online version of the paper. Correspondence and requests for materials should be addressed to Q.X. (qihua@ntu.edu.sg).

Reviewer Information *Nature* thanks X. Cui and A. Malko for their contribution to the peer review of this work.

METHODS

Sample preparation. We used MoS_2 crystals (from 2D Semiconductors) and WS_2, WSe_2 and $MoSe_2$ crystals (from HQ Graphene) for mechanical exfoliation, and we transferred and aligned 2D monolayer pieces with a solvent-free procedure. For instance, to achieve a $WS_2/MoSe_2$ heterostructure, we used a blue tape for repeated exfoliation of a piece of bulk crystal and then stuck the tape (with exfoliated crystal pieces) onto a PDMS layer (PF-X4, Gel-Pack). The assembly was held in vacuum for 2 hours to achieve a better contact, and then the blue tape was removed, leaving monolayer WS_2 or $MoSe_2$ on a PDMS layer. The WS_2/PDMS film was put onto a SiO_2 (80 nm)/Si substrate cleaned by oxygen plasma; then the PDMS was removed, leaving monolayer WS_2 on SiO_2/Si. $MoSe_2$/PDMS film was then attached exactly to WS_2/SiO_2/Si (after careful alignment with a XYZ manipulation stage under an optical microscope) and held in vacuum for 2 hours. The top PDMS layer was then removed, resulting in a $WS_2/MoSe_2$ bilayer heterostructure on the substrate. Similar approaches can be applied to any TMD combinations to achieve various heterostructures. All measurements were implemented at room temperature and under ambient conditions if not otherwise noted.

Dynamical fluorescence imaging. We used a Photron FASTCAM SA1.1 monochrome high-speed camera to record dynamical variation in emission, with the sample illuminated with an Olympus U-HGLGPS lamp (130 W output) after passing through a 477-nm bandpass filter ($\sim$17 mW under a $\times$100 objective). Bandpass filters of 645/75 nm, 747/33 nm and 794/34 nm (from Semrock) were used to selectively extract luminescence information from WS_2, WSe_2 and $MoSe_2$, respectively. Videos were recorded at a speed of 125 frames per second and with an 8-ms exposure time for each frame. Time traces were calculated from the grey scale of regions of interest from each frame.

Transient absorption spectroscopy. We carried out pump–probe measurements using a home-built system based on a mode-locked Ti:sapphire laser. The direct-diode-pumped Ti:sapphire laser oscillator provides a 13-fs pulse width with a repetition rate of 64 MHz. The output of the laser is split into two parts: the small portion serves as the probe beam; the second part is spectrally manipulated in a grating-based 4f-shaper with the purpose of providing an independently tunable centre wavelength and spectral bandwidth of the pump pulse (typical pulse width 60 fs). Both beams are non-collinearly focused on the sample by means of an off-axis parabolic mirror, achieving focal diameters of 4 μm and 10 μm for probe and pump beams, respectively. We used a long-working-distance objective (Mitutoyo, APO Plan NIR HR $\times$100) for sample imaging as well as for collection of the transmitted probe beam. The probe was then refocused onto an entrance slit of an aberration-reduced imaging spectrometer (Princeton Instruments IsoPlane-320). We used a mechanical chopper with a synchronized readout from a liquid-nitrogen-cooled charge-coupled-device (CCD) camera (Princeton Instruments Pylon) for acquisition of probe spectra with and without pump-induced changes, enabling calculation of a relative differential transmission. All of the pump–probe measurements were conducted under ambient conditions at room temperature, and the pump spectrum was adjusted to cover a wavelength range of 810 nm to 845 nm. The data in Fig. 2f, g were acquired with average pump powers of 1.3 mW and 5 mW, respectively. The average power of the probe beam is set to 30 μW for all of the reported measurements.

Steady-state and transient fluorescence spectroscopy. Emission spectra were measured with a Horiba HR Evo spectrometer (with a focal length of 800 mm), equipped with a 300 lines mm^{-1} grating and a 1,024-pixel CCD detector, corresponding to a spectral resolution of $\Delta E = 0.34$ meV at 620 nm. We used a 150 lines mm^{-1} grating to collect the spectra from WS_2 and $MoSe_2$ simultaneously, for the correlation studies shown in Fig. 4. The excitation wavelength was 532 nm with a power of $\sim$1.5 μW (30 μW for Fig. 4a and 15 μW for Fig. 3e, f, to allow a shorter exposure time). Time traces were acquired with a Nikon $\times$50 long-working-distance objective (numerical aperture = 0.45); the incident laser was defocused slightly to illuminate the whole heterostructure. We do observe brighter emission in the fluorescence microscopy at a different time, as shown in Supplementary Video 3; the emission spectra shown in Fig. 3a–d are all weaker than that for pristine WS_2, possibly because of practical limitations in terms of exposure time and because of blinking kinetics. We used Labspec 6 software for batch fitting analysis, to obtain integrated intensity and emission-energy information. For correlation and lifetime analysis, we used a Ti:sapphire femtosecond-pulsed laser (800 nm, 80 MHz, $\sim$100 fs) that was frequency-doubled by a beta barium boron crystal, to generate 400-nm pulsed laser for excitation. We used a 750-nm short-pass filter to remove the 800-nm incident laser. Signal was collected with a $\times$100 objective (Nikon, numerical aperture = 0.90) using a back-scattering mode. After removing the 400-nm laser with a 532-nm long-pass filter, we divided the signal beam into two paths with a 50/50 beam splitter, while measuring the signals of the two beams with two SPAD detectors. The instrument-response function of our system is shown in Supplementary Fig. 12, and it can be fitted with a Gaussian function yielding a full-width at half-maximum of 53 ps. For correlation experiments with a $WS_2/MoSe_2$ heterostructure, we used 645-nm and 794-nm bandpass filters to extract the emission signals from WS_2 and $MoSe_2$, separately. To generate the cross-correlation function $G(\tau)$, we took $I_{WS_2}(t)$ and $I_{MoSe_2}(t)$—the emission intensities from the two components at time t as shown in Fig.4g. Angular brackets denote averaging over time. $\delta I_{WS_2}(t) = I_{WS_2}(t) - \langle I_{WS_2}(t)\rangle$ gives intensity fluctuations in WS_2 emission. Single-photon counting was performed with a PicoHarp 300 module (PicoQuant). To generate statistics for ON/neutral/OFF states, we defined the ON and OFF thresholds to be $I+3\sigma$ and $I-3\sigma$ respectively, where I is the signal intensity with the largest occurrence in the signal level distribution and σ is the standard deviation of the SPAD background counts. For intensities in the range $(I-3\sigma, I+3\sigma)$, we defined the state as neutral. We analysed data using SymPhoTime 64 software.